Wiley Analytical Science



Automating the Laboratory: Maximizing Efficiency Through Smart Solutions

April 27, 9:00am - 10:00am EDT

Automation has reached ever larger areas recently. Due to the development of numerous new, cost-effective automation devices and modules, the automation of laboratory processes is also of increasing interest to small and medium-sized companies and research laboratories. Different degrees of automation from the automation of individual sub-steps to partial automation and finally full automation without manual intervention by an operator are possible.

Watch this session during the WAS Virtual Conference:



Prof. Kerstin Thurow



Prof. Thole Züchner

Register Now

This talk is sponsored by SARTORIUS

Research Article Wiley Online Library ELECTROANALYSIS

doi.org/10.1002/elan.202200182

Electrochemical Behavior and Ultrasensitive, Simple and Effective Voltammetric Determination of Acetaminophen Using Modified Glassy Carbon Electrode Based on 4-Hydroxyquinoline-3-carboxylic Acid

Demet Uzun*[a] and Tuğba Tabanlıgil Calam[b]

Abstract: An electrochemical oxidation of acetaminophen (ACOP) has been successfully performed by using glassy carbon electrode covered with 4-hydroxyquinoline-3-carboxylic acid (4HQ3CA) to reinforce electrode's feature. To characterize the modified electrode (4HQ3CA/GC), electrochemical impedance spectroscopy (EIS), cyclic voltammetry (CV) and Fourier transform infrared spectroscopy (FT-IR) techniques were used. The finding optimum conditions (supporting electrolyte, pH) and the electrochemical determination studies were performed with differential pulse voltammetry (DPV). It was decided that the supporting electrolyte medium suitable for ACOP determination was Britton-Robinson (BR) buffer and the effect of pH change on the oxidation peak of ACOP in this media was investigated. The effect of changing scan rate on the oxidation peak of ACOP was examined and this study showed that the oxidation process of ACOP on the 4HQ3CA/GC modified electrode surface was diffusion and adsorption controlled process. A wide concentration range from 0.0025 μM to 141 μM with a limit of detection (LOD) of 5.98×10^{-10} M (3 s/m) was obtained. This prepared sensor was carried out for the determination of ACOP in pharmaceutical sample.

Keywords: Determination · modification · acetaminophen · pharmaceutical sample · voltammetry

1 Introduction

ACOP (acetaminophen, paracetamol, 4-acetamidophenol, N-acetyl-p-aminophenol) has been widely used as an antipyretic and analgesic drug for more than 50 years in the world [1]. ACOP is used to relieve muscle aches, migraine headaches, and chronic pain, as well as reduce fever and relieve discomfort caused by colds [2]. In addition, the use of ACOP as a drug has almost replaced the use of aspirin for aspirin-sensitive individuals and to avoid the risk of Reye's syndrome in infants [3]. Furthermore, it is helpful in osteoarthritis therapy and is preferred as an analgesic drug for asthma patients [4,5]. Medical studies have shown that ACOP may offer some protection against ovarian cancer [6]. In addition, recent research has shown that ACOP may be effective in protecting against the hardening of the arteries that cause cardiovascular disease [7]. ACOP is not carcinogenic.

Limited use of ACOP is safe and does not exhibit any side effects [8]. However, chronic or overdose of ACOP can result in liver and kidney damage in some cases and even coma or death [3,9]. However, in terms of contributing to clinical diagnosis and drug quality control, developing analytical techniques is important for the sensitive determination of ACOP [2,9]. Therefore, development of a novel, accurate, sensitive, simple analytical method for the determination of ACOP is important. To this end, numerous techniques were used for the detection of ACOP in biological samples and drug formulations. The used most commonly techniques to determine the concentration of ACOP were spectrophotometry [10,11], high performance liquid chromatography (HPLC) [12], HPLC with a fluorescence detector [13], HPLC with a NMR-MS [14], HPLC with a GC-MS [15,16], HPLC with a UV–Vis detector [17–19], chemiluminescence [20], capillaryelectrophoresis (CE) [21], UV–Vis spectrophotometry [22], titrimetry [23]. However, most of these techniques have several disadvantages such as a pretreatment requirement before determination, high cost of apparatus, being time-consuming [24]. Alternatively, the electrochemical techniques are preferred due to their high accuracy, precision, selectivity and sensitivity, simple and low-cost instrumentation, rapid response [25–27]. Also, the electrochemical techniques usually do not require a pretreatment process [28–30]. For the determination of ACOP in pharmaceutical samples, especially voltammetric techniques are widely used because they are more sensitive, selective and sensitive [31]. In recent years,

[a] D. Uzun
Gazi University, Science Faculty, Department of Chemistry, 06500 Ankara, Turkey
Tel: +90 312 2021497; Fax: +90 312 2122279
E-mail: demetuzun@gazi.edu.tr
[b] T. Tabanlıgil Calam
Gazi University, Technical Sciences Vocational High School, Department of Chemical Technology, 06500 Ankara, Turkey

 © 2022 Wiley-VCH GmbH

surface modification studies have become important in order to increase the analytical performance for the sensitive determination of the target species. Uzun coated glassy carbon (GC) electrode with a triazole derivative [9]. The determination of ACOP was performed with this prepared electrode by differential pulse voltammetry (DPV) in a pharmaceutical sample [9]. Tabanlıgil Calam carried out the determination of ACOP using a modified electrode based on 3,5-diamino-1,2,4-triazole polymer film on the GC electrode [2].

A wide variety of materials such as inorganic/organic molecules, nanoparticles, carbon nanotubes and graphene have been used to modify the solid electrode surface. Hasan et al. modified carbon paste electrode with iron oxide nanoparticles for the determination of ACOP [32]. Kareem et al. modified the GC electrode surface with multiwalled carbon nanotube (MWCNT/GC) and graphene (graphene/GC) to study the electrochemical behaviour of ACOP using the CV technique [33]. However, the use of these materials for the modification process both increases the cost and increases the preparation time of the modified electrode.

In this study, a novel electrochemical sensor named as 4HQ3CA/GC was fabricated with 4-hydroxyquinoline-3-carboxylic acid by CV technique. The developed electrode was prepared with an easy and fast process. The 4HQ3CA/GC electrode was characterized using redox probes by the CV and EIS techniques. Also, the surface characterization was performed by using FT-IR and SEM, and the surface property of 4HQ3CA/GC was compared with bare GC. The coating of the GC surface with 4HQ3CA molecule (Figure 1 inset) containing carboxylic acid and hydroxide groups attached to the aromatic ring caused the oxidation peak current of ACOP to increase significantly. Sensitive voltammetric determination and electrochemical behavior of ACOP were performed with the 4HQ3CA/GC sensor. For the determination of ACOP, the sensor exhibited a good analytical performance with a LOD and a wide linear range. Also, high accuracy and good precision results were get on the 4HQ3CA/GC electrode for the electrooxidation of ACOP in pharmaceutical samples. The peak potential was located around 0.5–0.6 V for ACOP on the 4HQ3CA/GC electrode. Although generally many interferents also produce electrochemical signals in this area, the selectivity of this sensor is still good. This is the biggest advantage of this produced sensor.

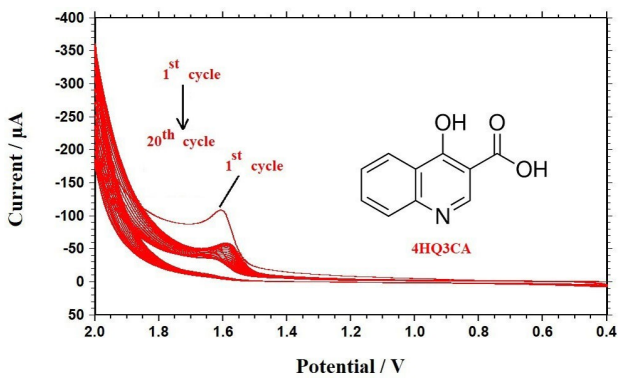


Fig. 1. Multiple cyclic voltammograms showing the electrochemical deposition of 1×10^{-3} M 4HQ3CA prepared with 0.1 M H_2SO_4 solution on the GC electrode surface.

2 Experimental

2.1 Reagents and Apparatus

4HQ3CA, perchloric acid (70 %, $HClO_4$), potassium chloride (KCl) and phosphoric acid (85 %, H_3PO_4) were provided from Sigma-Aldrich (Germany). ACOP, sulphuric acid (97 %, H_2SO_4), sodium hydroxide, sodium acetate (NaAc), potassium ferrocyanide ($K_4[Fe(CN)_6]$), acetonitrile (ACN, chromatographic grade), sodium phosphate dibasic, potassium ferricyanide ($K_3[Fe(CN)_6]$), sodium phosphate monobasic, acetic acid (HAc, glacial), ferrocene, tetrabutylammonium tetrafluoroborate (TBATFB) and boric acid (H_3BO_3) were obtained from Merck (Germany). 1×10^{-3} M 4HQ3CA solution was prepared in the 0.1 M H_2SO_4 solution. The stock solution of ACOP (1×10^{-3} M) was daily prepared in double-distilled water. All chemicals were analytical reagent grade. Ferrocene solution as the anhydrous medium was prepared in ACN containing 0.1 M TBATFB. Other solutions were prepared using double-distilled water.

Stock BR solution (1.0 L, 0.04 mol L^{-1}) was prepared by mixing together 2.70 mL of H_3PO_4, 2.30 mL of HAc and 2.47 g of H_3BO_3 and enough double-distilled water. The pH adjustment of the BR buffer taken in certain amounts was made using 2.0 mol L^{-1} HCl and 2.0 mol L^{-1} NaOH solutions.

All electrochemical measurements (CV, DPV and EIS) were performed with CHI 660B electrochemical workstation (CH Instruments, China) with a three-electrode system. For all electrochemical measurement, a covered GC (BASi, MF-2012, USA) as the working electrode, a Ag/AgCl/KCl (sat.) (silver/silver chloride, BASi, MW-2021, USA) as the reference electrode in aqueous medium and a Pt wire (platinum, BASi, MW-1032, USA) as the counter electrode were used. In nonaqueous medium measurements, Ag/Ag^+ (silver/silver nitrate, BASi, MF-2062, USA) was used as the reference electrode. This reference electrode was prepared with 0.01 mol L^{-1} Ag^+ in ACN solution containing 0.1 mol L^{-1} of TBATFB. All experimental measurements were carried out at room temperature.

To obtain FT-IR spectra, a Thermo Fisher Scientific brand spectrophotometer (Nicolet IS5 model, US) was used. It contains ATR with KBr pellet head and diamond lens. In order to examine the morphological properties of modified and bare electrode surfaces and compare them with each other, a JEOL brand JSM-6060 LV model SEM (USA) was used at 0.5–30 kV. A GC disc electrode was used for FT-IR and SEM measurements.

 © 2022 Wiley-VCH GmbH

15214109, 2023, 4, Downloaded from https://analyticalsciencejournals.onlinelibrary.wiley.com/doi/10.1002/elan.202200182 by Gazi University, Wiley Online Library on [26/04/2023]. See the Terms and Conditions (https://onlinelibrary.wiley.com/terms-and-conditions) on Wiley Online Library for rules of use; OA articles are governed by the applicable Creative Commons License

2.2 Preparation of Modified Electrode

The GC electrode surfaces were firstly polished with 0.05 μm alumina slurry on the microcloth pads, after these were sonicated for 15 min and rinsed with double-distilled water, and dry at ambient temperature. As seen in Figure 1, the modification of GC surface was performed with 1×10^{-3} M 4HQ3CA solution in 0.1 M H_2SO_4 using CV with 100 mVs^{-1} scan rate for 20 cycles between +0.4 V and +2.0 V.

2.3 Electrochemical Determination using 4HQ3CA Modified GC

The determination of ACOP was performed on the 4HQ3CA/GC electrode at pH 1.0 in BR buffer as supporting electrolyte using the DPV technique at room temperature. All DPV measurements were performed in the potential range from +0.3 to +0.9 V with a 0.05 s of pulse width, 0.2 s of pulse period and 0.10 V of wave amplitude.

2.4 Preparation of Real Sample to Determine ACOP

The 4HQ3CA/GC sensor was fabricated to the determination of ACOP in the pharmaceutical product. The pharmaceutical product as effervescent tablet was supplied from a pharmacy. The effervescent tablet is sold as a cold medicine containing acetylsalicylic acid, caffeine, and ACOP. The taken effervescent tablet was solved in 100 mL pure water. The sample solutions were prepared at 0.099, 1.10 and 11.00 μM concentrations by adding different volumes of this sample into the electrochemical cell containing 10 mL of supporting electrolyte. Then, known concentrations of ACOP were added to the electrochemical cell. The concentration of ACOP was detected using the standard addition method with three repetitive measurements by the DPV method.

3 Results and Discussion

3.1 Development of the Modified Electrode

The multi-cyclic voltammograms (CVs) of 4HQ3CA on the GC electrode were obtained with 20 cycles to prepare 4HQ3CA/GC electrode. A characteristic irreversible anodic peak was seen at +1.6 V potential in the first cycle in CVs in Figure 1, and with the second cycle, the peak potential shifted slightly to negative. The anodic peak current gradually decreased with increasing cycles numbers. The decrement of a peak current and the shift of peak potential showed a fabricated of the 4HQ3CA film on the GC surface with the increasing potential cycle [34].

3.2 The Electrochemical Characterization of 4HQ3CA/GC and by Cyclic Numbers on the Preparation of 2–4HQ3CA/GC

The electrochemical tests for the bare and modified electrodes were carried out using ferricyanide/ferrocyanide ($[Fe(CN)_6]^{3-/4-}$) and ferrocene redox probes. Both surface characterization can be made and the number of coatings can be determined by this electrochemical tests. The electrocatalytic property of GC is dependent on thickness of the film [35,36]. The effect of different cycle numbers (15, 20, 25 and 30) on the coating was studied in a mixture of 1 mM $[Fe(CN)_6]^{3-/4-}$ and 1 mM ferrocene prepared in 0.1 M KCl and in ACN containing 0.1 M TBATFB, respectively. The CVs of $[Fe(CN)_6]^{3-/4-}$ and ferrocene on the coated electrode with different multiple cycles and bare GC were given in Figure 2a and Figure 2b. Figure 2 demonstrated that the reduction and oxidation peaks relevant to the redox probes slightly disappeared and blocked with increasing cycle numbers. This case is probably due to the blocking of electron transfer at the 4HQ3CA/GC electrode in both aqueous and non-aqueous medium. The blocking was almost completed at 20 CV, which is the reason why the optimum number of coating cycles was chosen as 20 CV.

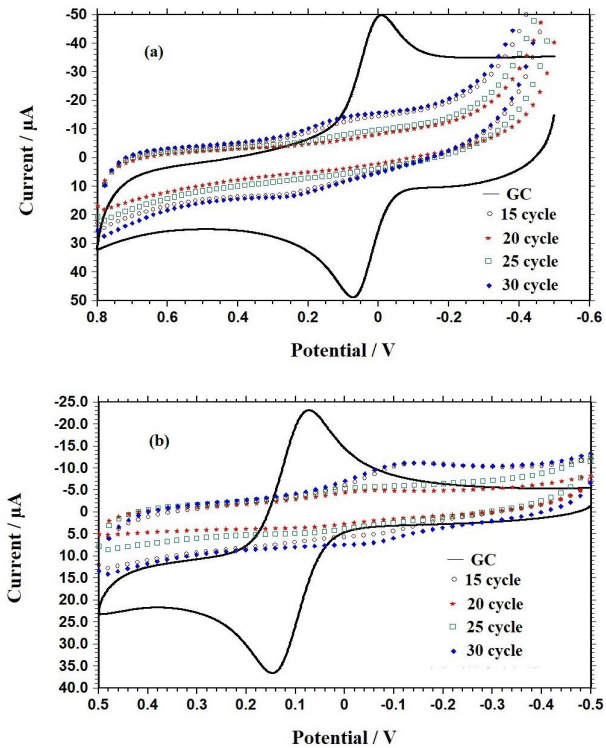


Fig. 2. CVs of 1 mM (a) $[Fe(CN)_6]^{3-/4-}$ (in the aqueous media) and (b) ferrocene (in an anhydrous media) on 4HQ3CA/GC electrode surface prepared with different cycle numbers (scan rate is 100 mVs^{-1}).

 © 2022 Wiley-VCH GmbH

15214109, 2023, 4, Downloaded from https://analyticalsciencejournals.onlinelibrary.wiley.com/doi/10.1002/elan.202200182 by Gazi University, Wiley Online Library on [26/04/2023]. See the Terms and Conditions (https://onlinelibrary.wiley.com/terms-and-conditions) on Wiley Online Library for rules of use; OA articles are governed by the applicable Creative Commons License

3.3 Characterization of Modified Electrode by EIS

EIS is a powerful tool and an alternating current (AC) technique to characterize of the electric features of the electrode surfaces [37]. It provides to study chemical and physical processes in solutions as well as in solids. A periodic small amplitude signal is applied by this technique to follow the electrical current response of the working system [38]. The electrochemical impedance spectra inform significant physical information about the features of the interface such as capacitance, resistance, etc., but for the detailed data, it is essential to use modelling called as equivalent electrical circuit [37]. The experimental spectra can be fitted using equivalent circuits to obtain values of electrical parameters that are directly related to the electrochemical process occurring at the electrode surface.

The impedance measurements were performed at a potential of 0.215 V in the frequency range from 0.05 Hz to 100 kHz versus Ag/AgCl. The AC amplitude was 5 mV. The Randle's equivalent circuit was used to model the Nyquist plots. Data fitting and electrochemical simulations were carried out using the CHI 660 B software. The EIS results of the bare GC (curve a) and 4HQ3CA/GC (curve b) in the presence of equimolar redox couple (5 mM, $[Fe(CN)_6]^{3-/4-}$) containing 0.1 M KCl have been studied, respectively. EIS curve observed at the bare GC included a semicircle part and a linear part at high and low frequencies, respectively. This linear part of the curve is related to the diffusion process and the semicircle part of the curve is related to the limited electron transfer process. For the bare and modified electrodes, the electrode/solution interface was modeled with the fitting equivalent circuits as shown in Figure 3(a) and (b), respectively. In the circuits, the charge-transfer resistance is Rct, the solution resistance between the reference and working electrodes is Rs, the double-layer capacitance in parallel with Rct is Qdl, and the Warburg resistance is W.

As can be seen in Figure 3, the Rct value was about 60.00 ohm on the bare GC. After being modified with 4HQ3CA film, the Rct value increased dramatically to about 6.569×10^4 ohm (4HQ3CA/GC). The increased Rct value in the electrode modification process indicated that the 4HQ3CA film was coated on GC surface and also hindered the charge transfer. This may be because the surface charge is negative and an electrostatic repulsion occurs between the surface and $[Fe(CN)_6]^{3-/4-}$. The values of the equivalent circuit elements for bare and modified electrodes were as shown in Table 1.

The percent electrode coverage value of the modified electrode, indicated by θ, was calculated using the formula $\theta\% = (1-Rct^0/Rct) \times 100$. In this formula, the charge-transfer resistance of bare GC and 4HQ3CA/GC modified electrode are Rct^0 and Rct, respectively. The value of percent electrode coverage was found as 99.91 % from the above equation. This showed that the permeability of the electrode surface decreased after the GC surface was covered by the 4HQ3CA film.

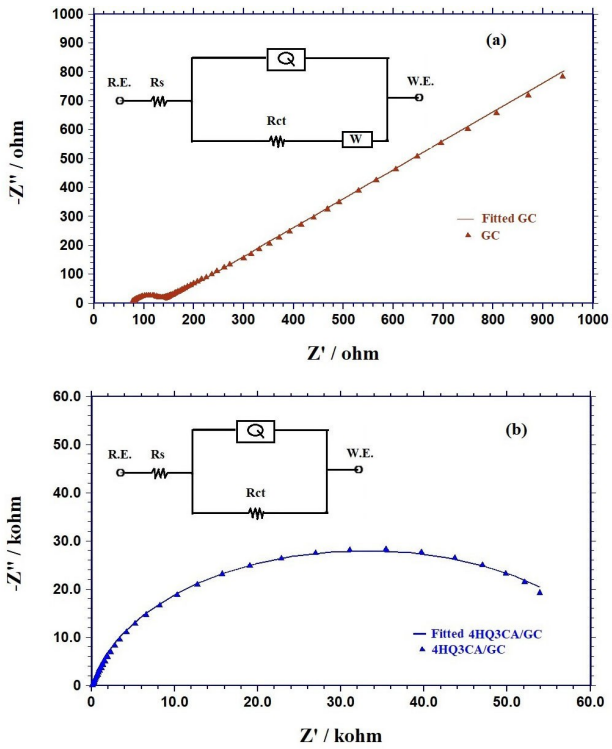


Fig. 3. Nyquist plots for (a) bare GC and (b) 4HQ3CA/GC with the Randle's equivalent circuit models for GC and 4HQ3CA/GC.

Table 1. Impedance parameters for the GC and 4HQ3CA/GC surfaces.

The Randle's Equivalent Circuit Elements	Bare GC	4HQ3CA/GC
Rs (ohm)	79.0	83.5
Q (μS)	0.185	15.95
n	0.995	0.898
Rct (ohm)	60.00	65690
W(mS)	1.481	–

3.4 The Analysis of 4HQ3CA/GC by FT-IR Measurement

FT-IR measurements were used to characterize 4HQ3CA/GC and investigate the binding sites of the 4HQ3CA film to the GC surface [39]. Bare GC electrode surface spectra were obtained and taken away from the modified surface spectra to get the film spectra of the grafted 4HQ3CA. The FT-IR spectrum of bare GC was as shown at the bottom on the left-hand side in Figure 4. Spectra of solid 4HQ3CA and 4HQ3CA film were given by the a and b curves in Fig.4, respectively. The differences between 4HQ3CA film on the GC surface and solid 4HQ3CA were determined with comparing the main IR bands of them. When curve a and curve b were compared given in Figure 4, for the 4HQ3CA film on the GC

 © 2022 Wiley-VCH GmbH

15214109, 2023, 4, Downloaded from https://analyticalsciencejournals.onlinelibrary.wiley.com/doi/10.1002/elan.202200182 by Gazi University, Wiley Online Library on [26/04/2023]. See the Terms and Conditions (https://onlinelibrary.wiley.com/terms-and-conditions) on Wiley Online Library for rules of use; OA articles are governed by the applicable Creative Commons License

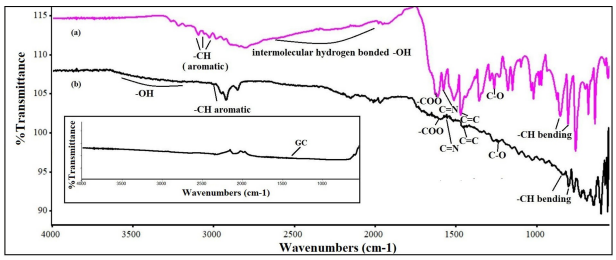


Fig. 4. FTIR spectra of (a) solid 4HQ3CA and (b) 4HQ3CA film on the GC. The spectrum belongs to bare GC was given at the bottom of left in Figure 4.

surface, the bands related to O–H stretching were seen as a broadband at 3653–3128 cm^{-1}. But these bands were not observed in this region for solid 4HQ3CA. But, the broad bands observed in the region 2768–2100 cm^{-1} for the solid 4HQ3CA showed the presence of the intermolecular hydrogen bonded O–H stretching vibrations with carboxylic OH groups. CH stretching (aromatic) vibrations of aromatic compounds are mostly seen as multiple weak bands in the 3100–3000 cm^{-1} region [40]. The spectrum belongs to solid 4HQ3CA gives the C–H stretching modes of the phenyl ring at 3102, 3064, 3035 cm^{-1}. These bands were not very well selected in the film spectrum may be due to orientation of 4HQ3CA to the surface. Only a weak band was observed at 3012 cm^{-1} belong to aromatic band in the film spectrum. In the present work the infrared band observed at 1632 cm^{-1} was assigned to the stretching vibrations of COO– [41] for solid 4HQ3CA. This band was observed at 1606 cm^{-1} for the 4HQ3CA film and the intensity of this band was almost invisible at this point. This is probably due to the interactions between 4HQ3CA and GC surface. The stretching band belongs to C=C was seen at 1480 cm^{-1} for solid 4HQ3CA. This band appeared at 1460 cm^{-1} for 4HQ3CA film. The C=N stretching band was seen at 1583 cm^{-1} [42] for solid 4HQ3CA [40]. This band shifted to a low frequency region and appeared at 1558 cm^{-1} as a a weak band in 4HQ3CA film on the GC surface. The band observed at 1269 cm^{-1} was associated with the C–O band [43] for solid 4HQ3CA and it was shifted to 1246 cm^{-1} for 4HQ3CA film. The C–H bending groups were revealed by the peaks observed at 865 cm^{-1}, 812 cm^{-1} for solid 4HQ3CA while these groups were observed 840 cm^{-1}, 801 cm^{-1} for 4HQ3CA film, respectively. As a result, the shifting and the decreasing in frequency of some bands may evidence that 4HQ3CA is on the GC surface.

3.5 The Analysis of 4HQ3CA/GC by SEM

Information about the surface morphology of the electrode surfaces can be obtained by SEM measurements [44,45]. SEM images of bare and coated electrodes were given in Figure 5A and Figure 5B, respectively. It was clearly seen from these images that the surface morphology changed after the GC surface was covered with

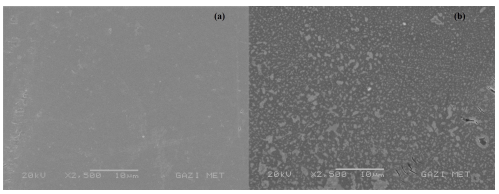


Fig. 5. SEM images of (a) bare GC and (b) 4HQ3CA/GC surfaces.

4HQ3CA film. In the enlarged SEM images of the bare GC, the GC surface appeared quite clean and smooth, while the random distribution of the 4HQ3CA film was uneven. This difference in the morphology of the bare GC and 4HQ3CA/GC electrode surfaces confirms that 4HQ3CA film has successfully attached to the surface of GC electrode.

3.6 Analytical Application of 4HQ3CA/GC as a Sensor of ACOP

3.6.1 The Effect of Supporting Electrolyte and pH on the Oxidation of ACOP

The effect of supporting electrolyte and pH on the oxidation of ACOP was studied by using the DPV technique for the sensitive determination of ACOP. To this end, various supporting electrolyte solutions such as $HClO_4$ solution (pH 2.0) and H_2SO_4 solution (pH 2.0), HAc/NaAc buffer (ABS, pH 5.0), phosphate buffer (PBS, pH 5.0), BR buffer (pH 5.0 and 2.0) were used. The obtained voltammograms in these solutions were shown in Figure 6A. The anodic peak current values of 3×10^{-5} M ACOP in these medium were found as 1.81 μA, 2.18 μA, 1.81 μA, 3.98 μA, 1.71 μA and 4.22 μA, respectively. The highest peak current value of ACOP was obtained in the BR solution. This is probably due to its composition that affects the electrode–solution interface modifying the thermodynamics and kinetics of the charge transfer process. Therefore, this medium was chosen as the supporting electrolyte solution to sensitive determine ACOP.

The effect of pH on the current and potential of the oxidation peak of ACOP was investigated. Voltammograms obtained in the pH range of 1.0–5.0 of the BR buffer were shown in Figure 6B. The maximum value of anodic peak current of ACOP was obtained at pH 1.0 in BR buffer solution. Therefore, it was seen that suitable supporting electrolyte medium was pH 1.0 BR buffer solution for the detection of ACOP. Also, the oxidation peak potential values changed with changing pH values. The graph shown in Figure 6C showed the linear relationship between potential and pH values. The equation of this line with a slope value of −45.0 mV pH^{-1} was obtained as $Ep = -0.0450pH + 0.5928$ ($R^2 = 0.9973$). This slope value indicated the same number of protons and electrons took part for the oxidation process of ACOP.

 © 2022 Wiley-VCH GmbH

15214109, 2023, 4, Downloaded from https://analyticalsciencejournals.onlinelibrary.wiley.com/doi/10.1002/elan.202200182 by Gazi University, Wiley Online Library on [26/04/2023]. See the Terms and Conditions (https://onlinelibrary.wiley.com/terms-and-conditions) on Wiley Online Library for rules of use; OA articles are governed by the applicable Creative Commons License

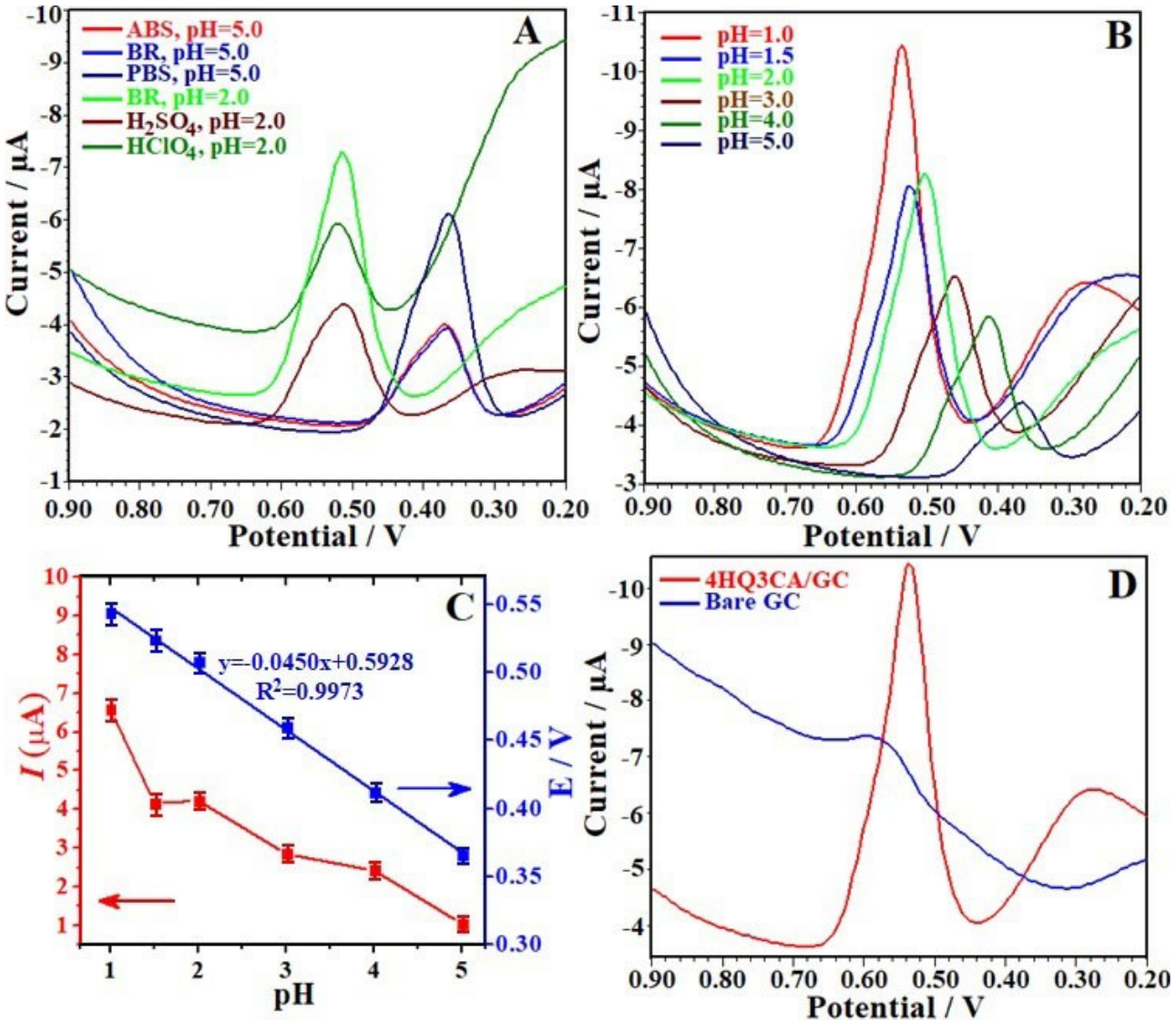


Fig. 6. A. DPVs of 3×10^{-5} M ACOP in different supporting electrolyte medium (ABS, PBS and BR buffers; H_2SO_4 ve $HClO_4$ solutions), B. DPVs of 3×10^{-5} M ACOP in different pH values of BR buffer, C. Plot of oxidation peak potential and current values of 3×10^{-5} M ACOP versus pH values of BR buffer, D. DPVs of 3×10^{-5} M ACOP in BR buffer solution at pH 1.0 on the bare GC and 4HQ3CA modified electrode.

The ratio of the numbers of proton (m) to the number of electron (n) was found using Equation 1. Also, F is the Faraday constant (96485 C mol^{-1}), T is the temperature (298.15 K) in Equation 1.

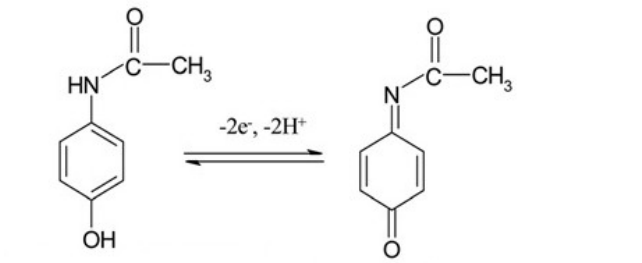
$$\frac{dEp}{dpH} = \frac{2.303mRT}{nF} \quad (1)$$

The value of the ratio of the numbers of proton (m) to the number of electron (m/n) for the oxidation of ACOP was calculated to be 0.76 (about 1). This result showed that the number of electrons and protons transferred in the oxidation process of ACOP are equal each other. In addition, it was reported that the number of transferred electrons is 2 in the oxidation process of ACOP in the literature [46,47]. Based on these results, the possible oxidation mechanism of ACOP on the 4HQ3CA/GC modified electrode surface was suggested as shown in Scheme 1.

The DPVs of 3×10^{-5} M ACOP at pH 1.0 in BR buffer on bare GC and 4HQ3CA/GC were shown in Figure 6D. The oxidation peak current values of ACOP on the bare GC and 4HQ3CA/GC electrodes were obtained as 0.79 and 6.50 µA, respectively. The peak current value on the 4HQ3CA/GC modified electrode was about 8.23 times larger than the peak current value on the bare GC. It can be seen from the DPV voltammograms (Figure 6D), the oxidation peak potantial was shifted to less positive potential direction at the modified electrode compared with the bare GC. These result clearly remarks that the 4HQ3CA/GC improve electron transfer reaction for the oxidation of ACOP.

 © 2022 Wiley-VCH GmbH

15214109, 2023, 4, Downloaded from https://analyticalsciencejournals.onlinelibrary.wiley.com/doi/10.1002/elan.202200182 by Gazi University, Wiley Online Library on [26/04/2023]. See the Terms and Conditions (https://onlinelibrary.wiley.com/terms-and-conditions) on Wiley Online Library for rules of use; OA articles are governed by the applicable Creative Commons License



Scheme 1. The oxidation mechanism of ACOP.

3.6.2 Effect of Potential Scan Rate on the Oxidation Peak of ACOP

The CV measurements were performed to investigate the kinetics of oxidation process of ACOP on the 4HQ3CA/GC electrode surface. For this purpose, the CVs of 3×10^{-5} M ACOP over the scan rate range of 0.025–0.4 $V s^{-1}$ (0.025, 0.05, 0.075, 0.10, 0.15, 0.20, 0.25, 0.30, 0.35 and 0.40 $V s^{-1}$) under the optimum conditions were obtained, and the voltammograms were showed in Figure 7A.

The graph in Figure 7B showed a linear relationship between the anodic peak current and the scan rate values. Equation of the plot of this relationship was found as $Ipa(\mu A)=8.3019v+0.4784$ ($R^2=0.9928$). This linearity

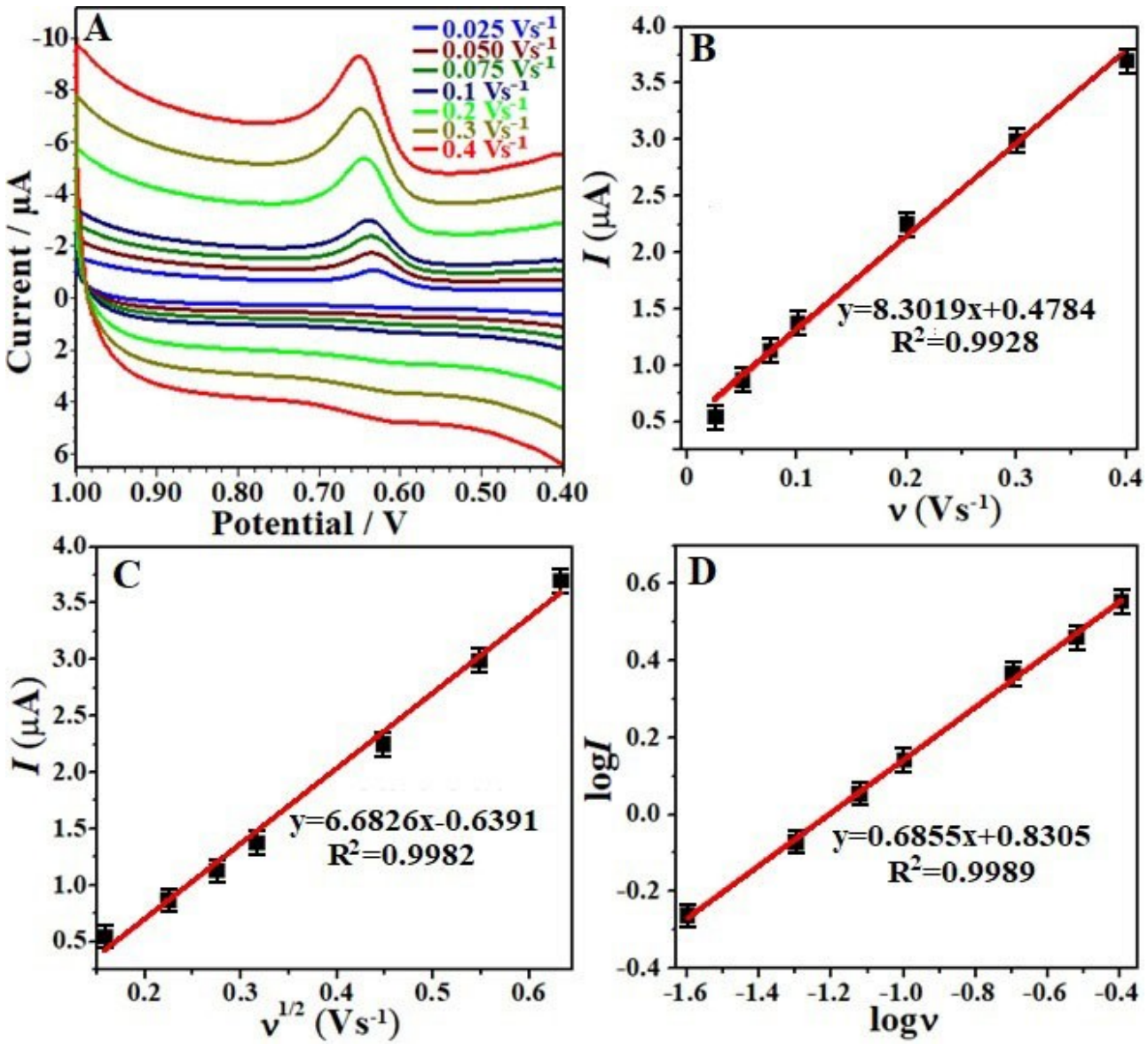


Fig. 7. A. CVs of 3×10^{-5} M ACOP with different scan rates on the 4HQ3CA/GC modified electrode surface in supporting electrolyte solution. B. The plot of I vs. v; C. The plot of I vs. $v^{1/2}$; D. The plot of logI vs. log$v$.

 © 2022 Wiley-VCH GmbH

15214109, 2023, 4, Downloaded from https://analyticalsciencejournals.onlinelibrary.wiley.com/doi/10.1002/elan.202200182 by Gazi University, Wiley Online Library on [26/04/2023]. See the Terms and Conditions (https://onlinelibrary.wiley.com/terms-and-conditions) on Wiley Online Library for rules of use; OA articles are governed by the applicable Creative Commons License

showed that the oxidation process of ACOP on the 4HQ3CA/GC surface was an adsorption-controlled [48].

A linear relationship between the anodic peak currents of ACOP and square root of scan rate was as seen in Figure 7C. Equation of this linear relationship was found as $Ipa(\mu A) = 6.6826v^{1/2} - 0.6391$ ($R^2 = 0.9983$). This result showed that the oxidation of ACOP on the 4HQ3CA/GC surface was diffusion-controlled process [49]. Also, the plot of the logarithm of anodic current against the logarithm of scan rate was as seen in Figure 7D. Equation of this linear relationship was found as $logIp(\mu A) = 0.6855logv + 0.8305$ ($R^2 = 0.9989$). The fact that the slope value found (0.6855) was between 0.5 and 1.0 theoretical values showed that the process of the process was both diffusion and adsorption controlled [50].

3.6.3 Calibration Graph, Limit of Detection and Linear Concentration Range

The analytical performance of 4HQ3CA/GC modified electrode for the voltammetric detection of ACOP was investigated by the DPV technique under the optimized conditions. For this purpose, ACOP was added in known concentrations and volumes to the electrochemical cell containing the supporting electrolyte. The oxidation peak currents of ACOP increased linearly with an increasing concentrations of ACOP. The voltammograms and calibration graph obtained with ACOP additions were shown in Figure 8A and Figure 8B, respectively. For the determination of ACOP, a wide operating range between 0.0025 μM and 141 μM (2.5 nM–141 μM) concentrations was obtained with the proposed sensor. The linear regression equation was found as $Ipa(\mu A) = 0.2206[ACOP](\mu M) - 0.0157$ ($R^2 = 0.9990$).

The values of LOQ and LOD were found with the equations 10 s/m and 3 s/m [51], respectively, where the slope of the analytical curve is m, and the standard deviation of the lowest concentration of the linearity range (n = 5) is s. For the voltammetric determination of ACOP with the proposed sensor, the LOQ and LOD values were found as 1.99×10^{-9} M and 5.98×10^{-10} M, respectively.

3.6.4 Comparison of the Reported Sensors in Literature with the Developed Sensor

The different sensors were reported for the voltammetric detection of ACOP in the literature. The linear working ranges and LOD values in some sensors in literature and proposed sensor were compared and were given in Table 2. The proposed sensor had a wider linear working range than most of the reported sensors in the literature for the detection of ACOP [2]. Also, the value of LOD obtained with the proposed sensor was lower than that of all reported sensors [2,9,52–60]. In addition, in view of the preparation processes of the other sensors given in Table 2, the ease of the 4H3CA/GC electrode preparation process provides so many advantages in terms of time savings.

3.6.5 Reproducibility, Repeatability, Selectivity and Stability of Sensor

Parameters as reproducibility, repeatability and selectivity of proposed sensor were investigated to determine the sensing performance of the sensor for the determination of ACOP. To investigate the reproducibility of sensor, a series of six modified electrodes were prepared with same

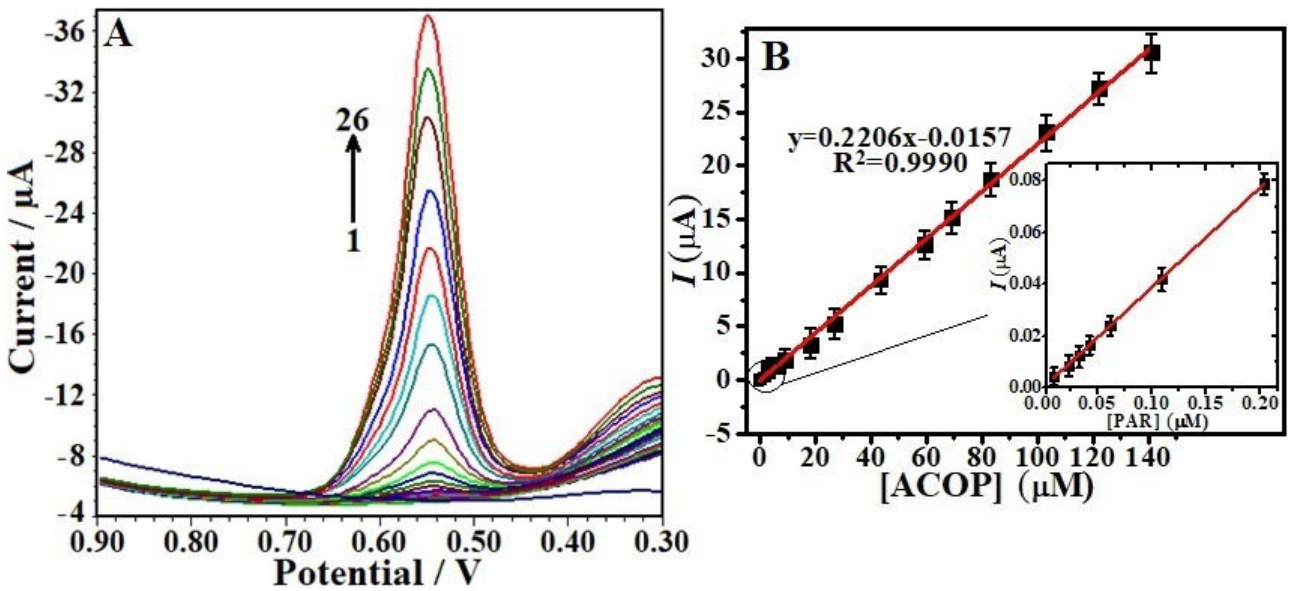


Fig. 8. **A)** DPVs of ACOP with different concentrations on the 4HQ3CA/GC surface in supporting electrolyte solution and **B)** the graph of calibration.

 © 2022 Wiley-VCH GmbH

15214109, 2023, 4, Downloaded from https://analyticalsciencejournals.onlinelibrary.wiley.com/doi/10.1002/elan.202200182 by Gazi University, Wiley Online Library on [26/04/2023]. See the Terms and Conditions (https://onlinelibrary.wiley.com/terms-and-conditions) on Wiley Online Library for rules of use; OA articles are governed by the applicable Creative Commons License

Table 2. Comparison of the LOD value and linear concentration range of the proposed method with some sensors in the literature.

Electrode	Linear range (μM)	LOD (μM)	Method	References
35DT[1]-GC[2]	0.30–55 and 55–475	0.1	DPV	[2]
3AT[3]-GC	0.108–14.2 and 14.2–89.5	0.043	DPV	[9]
PAY[4]-nanoTiO_2-GC	12–20	2	DPV	[52]
fMWCNT[5]-GC	1–90	0.52	DPV	[53]
PEDOT[6]-GO[7]-GC	10–60	0.57	CV	[54]
BDD[8]	0.5–83	0.49	DPV	[55]
AuNP[9]-MWCNT[10]-GC	0.09–35	0.03	DPV	[56]
NiONPs[11]-CB[12]-DHP[13]-GC	3–80	0.48	SWV	[57]
GO/Fe_3O_4@SiO_2/SPE[14]	0.5–100	0.1	DPV	[58]
Lcc[15]-TiO_2@CPE[16]	8–120	1	DPV	[59]
Co_1Ni_1@CN-700[17]/GC	0.05–40; 40–150	0.0038	DPV	[60]
4H3CA/GC	0.0025–141	0.000598	DPV	This study

[1]3,5-diamino-1,2,4-triazole, [2]Glassy carbon electrode, [3]3-amino-4H-1,2,4-triazole, [4]poly(acid yellow 9), [5]Functionalized multi-wall carbon nanotubes, [6]poly(3,4-ethylenedioxythiophene), [7]Graphene oxide, [8]Boron-doped diamond, [9]Gold nanoparticles, [10]Multi-walled carbon nanotubes, [11]Nickel oxide nanoparticles, [12]Carbon black, [13]Dihexadecylphosphate, [14]Screen-printed electrodes, [15]Laccase, [16]Carbon paste electrode, [17]Nitrogen-doped carbon coated CoNi alloy.

procedure. For obtained anodic peak currents of 3×10^{-5} M ACOP from DPV measurements, the value of RSD% was calculated as 4.54 % which indicates good reproducibility of proposed sensor. The repeatability of proposed sensor was studied by running twenty successive DPV measurements of 3×10^{-5} M ACOP. The DPV results provided excellent repeatability with RSD% of 1.71 %. For obtained anodic peak currents of 5×10^{-7} M ACOP (as low concentration) from DPV measurements, the value of RSD% was calculated as 4.82 % which indicates good reproducibility of proposed sensor. The repeatability of proposed sensor was studied by running twenty successive DPV measurements of 5×10^{-7} M ACOP. The DPV results provided excellent repeatability with RSD% of 3.24 %. The storage stability of the 4HQ3CA/GC electrode was also evaluated. The ACOP oxidation response current was measured after ten days storage at room temperature on air. The anodic peak current of ACOP on the 4HQ3CA/GC remained 92.3 % of its initial peak current value.

The DPV measurements of 3×10^{-5} M ACOP were get on the 4HQ3CA/GC surface in supporting electrolyte solution in the presence of possible interferences. It was seen from the obtained results that the effects of on ACOP oxidation of 1000-fold concentration (conc.) of Na^+, Ca^{2+}, K^+, Cl^-; 500-fold conc. of CO_3^{2-}, NO_3^-, glucose; 250-fold conc. of SO_3^{2-}; 200-fold conc. of sucrose; 150-fold conc. of caffein; 100-fold conc. of Zn^{2+} and CH_3COO^-; 30-fold conc. of 4-aminophenol; 5-fold conc. of acetylsalicylic acid were found to be less than 5 %. Table 3 showed the possible interference species, their tolerance ratio that did not cause more than 5 % change in the anodic peak current of ACOP, and the percentage changes in the anodic peak current of ACOP of the corresponding these. Based on these results, it was seen that the selectivity of the 4HQ3CA/GC sensor was good in the determination of ACOP.

Table 3. Interferences of various species on the anodic peak current of ACOP.

Coexisting substance	Tolerance Ratio*	Change of peak current%
Na^+	1000	−2.56
K^+	1000	−1.34
Ca^{2+}	1000	−4.09
Zn^{2+}	100	+3.83
Cl^-	1000	−2.15
CO_3^{2-}	500	−4.57
NO_3^-	500	−2.21
SO_3^{2-}	250	−2.52
CH_3COO^-	100	−4.33
Sucrose	200	+2.74
Glucose	500	+4.90
Caffein	150	−1.18
4-aminophenol	30	+4.57
Acetylsalicylic acid	5	+4.46
Dopamine	150	+2.73
Uric acid	50	+3.79
Ascorbic acid	250	+1.22

*Maximum ratio of species tested with the deviations below 5 %.

3.6.6 Real Sample Analysis

The pharmaceutical sample (the ACOP content is known) was added to the electrochemical cell along with the supporting electrolyte solution. Next, known volumes of ACOP solutions were added in the electrochemical cell, and the voltammograms obtained for each addition were recorded. The concentrations of ACOP in pharmaceutical samples prepared as 0.099, 1.10 μM and 11.00 μM were determined using DPV technique by the standard addition method for three replicate measurements. The concentrations of ACOP in these sample were found as 0.104, 1.12 μM and 10.82 μM, respectively. The measurement results is seen in Table 4. The values of RSD% were 4.81 %, 4.03 % and 1.02 %, and the values of recovery were 105.00 %, 101.51 % and 98.39 %, respectively. It is

 © 2022 Wiley-VCH GmbH

15214109, 2023, 4, Downloaded from https://analyticalsciencejournals.onlinelibrary.wiley.com/doi/10.1002/elan.202200182 by Gazi University, Wiley Online Library on [26/04/2023]. See the Terms and Conditions (https://onlinelibrary.wiley.com/terms-and-conditions) on Wiley Online Library for rules of use; OA articles are governed by the applicable Creative Commons License

Table 4. ACOP detection in pharmaceutical product using developed sensor.

Sample	Amount in sample (μM)	Amount and found (μM)	[b]RSD%	[c]Recovery%	t_{exp}	[d]t_{tab}
Tablet	0.099	0.104 ± 0.005	4.81	105.00	−1.73	2.92
	1.10	1.12 ± 0.045[a]	4.03	101.51	−0.77	2.92
	11.00	10.82 ± 0.11	1.02	98.39	2.83	2.92

[a]90 % confidence interval for 3 measurements, [b]RSD% was calculated as: S/X × 100, [c]Recovery% was calculated as: [C]found/[C]added × 100, [d]t_{exp}:calcuated t value; t_{tab} reported t value from Student t-test table with 95 % confidence level.

seen from these results that ACOP determination can be performed with good sensitivity and accuracy by using the 4HQ3CA/GC electrode in the pharmaceutical sample.

4 Conclusion

In the present study, a novel modified electrode as the sensor was prepared for the ultrasensitive determination of ACOP. The characterization of surfaces was performed by EIS, CV, SEM and FTIR techniques, and surface features of bare GC and 4HQ3CA/GC electrodes were compared with each other. For the determination of ACOP, the sensor displayed good analytical performance with a low LOD value and a wide working range. Also, the modified electrode demonstrated good repeatability, selectivity and reproducibility. The sensor in a real sample exhibited good precision and high accuracy for the detection of ACOP. This work presents a sensor with a low LOD value, which is easy, inexpensive, and can be prepared with a small number of steps, to determine ACOP over a wide operating range. In addition to all these advantages, the proposed sensor has demonstrated good repeatability, selectivity, stability, and reproducibility. For all these reasons, the 4HQ3CA/GC modified electrode is a good alternative to the other electrodes prepared and other methods used in the literature for the determination of ACOP.

Acknowledgements

This work has been supported by Gazi University Scientific Research Projects Coordination Unit under grant number “05/2019-22” and ID number “6557”.

Data Availability Statement

The authors confirm that the data supporting the findings of this study is available within the article.

References

[1] M. Jozwiak-Bebenista, J. Z. Nowak, *Acta Pol. Pharm.* **2014**, *71*, 11–23.
[2] T. Tabanlıgil Calam, *Electroanalysis* **2021**, *33*, 1049–1062.
[3] R. N. Goyal, V. K. Gupta, S. Chatterjee, *Sens. Actuators, B Chem.* **2010**, *149 (1)*, 252–258.
[4] K. Brandt, *Drugs* **2003**, *63*, 23–41.
[5] J. C. McCrae, E. E. Morrison, I. M. MacIntyre, J. W. Dear-and, D. J. Webb, *Br. J. Clin. Pharmacol.* **2018**, *842*, 218–2230.
[6] D. W. Cramer, B. L. Harlow, L. T. Ernstoff, K. Bohlke, W. R. Welch, E. R. Greenberg, *Lancet* **1998**, *35*, 104–107.
[7] A. A. Taylor, Baylor Ccollege of medicine-Abstract from Munich Meeting (Thirteenth IUPHAR Congress of Pharma-cology), **1998**.
[8] K. Annadurai, V. Sudha, G. Murugadoss, R. Thangamuthu, *J. Alloys Compd.* **2021**, *852*, 156911.
[9] D. Uzun, *Electroanalysis* **2021**, *33*, 1699–1706.
[10] M. Knochen, J. Giglio, B. F. Reis, *J. Pharm. Biomed. Anal.* **2003**, *33*, 191–197.
[11] F. Shihana, D. Dissanayake, P. Darga, A. Dawson, *Clin. Toxicol.* **2010**, *48*, 42–46.
[12] A. Marín, E. Garcıa, A. García, C. Barbas, *J. Pharmaceut. Biomed. Anal.* **2002**, *29*, 701–714.
[13] J. Meyer, U. Karst, *Chromatographia* **2001**, *54 (2001)*, 163–167.
[14] M. Spraul, A. S. Freund, R. E. Nast, R. S. Withers, W. E. Maas, O. Corcoran, *Anal. Chem.* **2003**, *75*, 1536–1541.
[15] T. Belal, T. Awad, R. Clark, *J. Chromatogr. Sci.* **2009**, *47*, 849–854.
[16] A. K. Hewavitharana, S. Lee, P. A. Dawson, D. Markovich, P. N. Shaw, *Anal. Biochem.* **2008**, *374*, 106–111.
[17] M. L. Altun, *Turk. J. Chem.* **2002**, *26*, 521–528.
[18] E. Pufal, M. Sykutera, G. Rochholz, H. W. Schütz, K. Sliwka, H. J Kaatsch, *J. Anal. Chem.* **2000**, *367*, 596–599.
[19] M. Kartal, *J. Pharm. Biomed. Anal.* **2001**, *26*, 857–864.
[20] D. Easwaramoorthy, Y. Yu, H. Huang, *Anal. Chim. Acta* **2001**, *439*, 95–100.
[21] A. Kunkel, S. Günter, H. Wätzig, *J. Chromatogr. A* **1997**, *768*, 125–133.
[22] A. R. Khaskheli, A. Shah, M. I. Bhanger, A. Niaz, S. Mahesar, *Spectrochim. Acta Part A: Mol. Biomol. Spectrosc.* **2007**, *68*, 747–751.
[23] K. G. Kumar, R. Letha, *J. Pharmaceut. Biomed. Anal.* **1997**, *15*, 1725–1728.
[24] N. T. A. Thu, H. V. Duc, N. Hai Phong, N. D. Cuong, N. T. V. Hoan, D. Quang Khieu, *J. Nanomaterials* **2018**, *2018*, 7619419.
[25] T. Tabanlıgil Calam, *Int. J. Environ. Anal. Chem.* **2019**, *99 (13)*, 1298–1312.
[26] T. Tabanlıgil Calam, *Food Chem.* **2020**, *328*, 1270982.
[27] G. Baysal, D. Uzun, E. Hasdemir, *J. Electroanal. Chem.* **2020**, *860*, 113893.
[28] T. Tabanlıgil Calam, D. Uzun, *Electroanalysis* **2019**, *31*, 2347–2358.
[29] F. En-Nakra, D. Uzun, E. Hasdemir, *J. Food Compos. Anal.* **2021**, *104*, 104183.
[30] T. Tabanlıgil Calam, *Microchem. J.* **2021**, *169*, 106557.
[31] R. M. Hanabaratti, S. M. Tuwar, S. T. Nandibewoor, J. I. Gowda, *Chem. Data Collect.* **2020**, *30*, 100540.
[32] I. M. A. Hasan, A. R. Tawfik, F. H. Assaf, *Russ. J. Electro-chem.* **2021**, *57 (5)*, 435–447.
[33] Z. N. Kareem, M. M. Radhi, A. A. Moosa, *IOP Conf. Ser.: Mater. Sci. Eng.* **2021**, *1105 (1)*, 012054.
[34] A.-L. Liu, S.-B. Zhang, W. Chen, X.-H. Lin, X.-H. Xia, *Biosens. Bioelectron.* **2008**, *23*, 1488–1495.
[35] P. S. Ganesh, B. K. Swamy, *J. Electroanal. Chem.* **2015**, *756*, 193–200.

 © 2022 Wiley-VCH GmbH

15214109, 2023, 4, Downloaded from https://analyticalsciencejournals.onlinelibrary.wiley.com/doi/10.1002/elan.202200182 by Gazi University, Wiley Online Library on [26/04/2023]. See the Terms and Conditions (https://onlinelibrary.wiley.com/terms-and-conditions) on Wiley Online Library for rules of use; OA articles are governed by the applicable Creative Commons License

[36] T. Tabanlıgil Calam, *J. Food Compos. Anal.* **2021**, *98*, 103809.
[37] Š. Skalová, V. Vyskočil, J. Barek, T. Navrátil, *Electroanalysis* **2018**, *30*, 207–219.
[38] W. Boumya, F. Laghrib, S. Lahrich, A. Farahi, M. Achak, M. Bakasse, M. A. El Mhammedi, *Heliyon* **2017**, *3*, e00392.
[39] T. Tabanlıgil Calam, E. B. Yılmaz, *Instrum. Sci. Technol.* **2021**, *49 (1)*, 1–20.
[40] R. Bhuvaneswari, K. Sakthi Murugesan, *Opt. Mater.* **2019**, *98*, 109431.
[41] G. Taşkın, O. Şanlı, G. Asman, *Appl. Surf. Sci.* **2011**, *257 (22)*, 9444–9450.
[42] V. M. Patel, N. B. Patel, M. J. Chan-Bacab, G. Rivera, *Comput. Biol. Chem.* **2018**, *76*, 264–274.
[43] G. Taşkın Çakıcı, O. Şanlı, *G. U. J. Sci, Part C* **2020**, *8 (3)*, 529–541.
[44] A. M. A Rahim, A. A. A. Gaber, E. M. M. Mahmoud, *Appl. Surf. Sci. Advances* **2020**, *2*, 100031.
[45] G. Asman, G. Taşkın Çakıcı, E. Kondolot Solak, K. Sivaprakasam, *G. U. J. Sci.* **2020**, *33 (1)*, 31–43.
[46] S. K. Hassaninejad-Darzi, F. Shajie, *Mater. Sci. Eng. C* **2018**, *91*, 64–77.
[47] J. Li, J. Liu, G. Tan, J. Jiang, S. Peng, M. Deng, D. Qian, Y. Feng, Y. Liu, *Biosens. Bioelectron.* **2014**, *54*, 468–475.
[48] Y. T. Yaman, G. Bolat, C. Yardımcı, S. Abacı, *Turk. J. Chem.* **2018**, *42*, 826–838.
[49] M. N. Ranku, G. E. Uwaya, O. E. Fayemi, *Molecules* **2021**, *26*, 5357.
[50] M. Amare, W. Teklay, *Cogent Chem.* **2019**, *5 (1)*, 1576349.
[51] T. T. Calam, G. T. Çakıcı, *J. Food Compos. Anal.* **2022**, *114*, 104728. .
[52] S. A. Kumar, C. Tang, S. Chen, *Talanta* **2008**, *76*, 997–1005.
[53] M. Baghayeri, M. Namadchian, *Electrochim. Acta* **2013**, *108*, 22–31.
[54] W. Si, W. Lei, Z. Han, Y. Zhang, Q. Hao, M. Xia, *Sensor. Actuat. B-Chem.* **2014**, *193*, 823–829.
[55] R. A. Medeiros, R. C. Rocha-filho, L. H. Mazo, O. Fatibello-Filho, *Talanta* **2009**, *78*, 748–752.
[56] T. Madrakian, E. Haghshenas, A. Afkhami, *Sensor. Actuat. B-Chem.* **2014**, *193*, 451–460.
[57] P. B. Deroco, C. Vicentini, O. Fatibello-filho, *Electroanalysis* **2015**, *27*, 2214–2220.
[58] H. Beitollahi, F. Garkani-nejad, S. Tajik, M. Reza, *Iran. J. Pharm. Res.* **2019**, *18*, 80–90.
[59] D. V. Thomaz, M. Teles de Oliveira, G. S. Lobón, C. E. P. da Cunha, F. B. Machado, E. K. G. Moreno, *Int. J. Electrochem. Sci.* **2018**, *13*, 10884–10893.
[60] X. Niu, X. Bo, L. Guo, *Anal. Chim. Acta* **2021**, *1145*, 37–45.

Received: April 18, 2022
Accepted: August 31, 2022
Published online on September 21, 2022

 © 2022 Wiley-VCH GmbH

15214109, 2023, 4, Downloaded from https://analyticalsciencejournals.onlinelibrary.wiley.com/doi/10.1002/elan.202200182 by Gazi University, Wiley Online Library on [26/04/2023]. See the Terms and Conditions (https://onlinelibrary.wiley.com/terms-and-conditions) on Wiley Online Library for rules of use; OA articles are governed by the applicable Creative Commons License